EPJ Web of Conferences **90**, 07002 (2015)
DOI: 10.1051/epjconf/ 20159007002

Impact of ATLAS measurements on PDFs

Nicola Orlando on behalf of the ATLAS Collaboration[1,a]

[1] *Aristotle University of Thessaloniki, Thessaloniki (GR); INFN–Lecce, Via Arnesano, Lecce (IT)*

Abstract. A review of the ATLAS measurements sensitive to parton distribution functions is presented. The analyses use proton–proton collision data at center–of–mass–energy $\sqrt{s}$ = 7 TeV collected at the Large Hadron Collider between April and November 2011. When included in QCD fits, the ATLAS data allow for improving the experimental constraints on the gluon and strange–quark parton density functions of the proton.

1 Introduction

The parton distribution functions (PDFs) are essential phenomenological ingredients for evaluating theory predictions of any observable at hadron collider experiments. They are introduced in the context of the Collinear Factorisation Theorem [1] as universal, namely process independent, kernels which "fold" the partonic cross sections and regularise the collinear singularity associated to the initial state radiation in perturbative Quantum–Chromo–Dynamic (pQCD).

The PDFs evolution as a function of the energy scale, Q^2, of the hard partonic process under investigation is calculated by solving the DGLAP equations in perturbative QCD. On the other hand, the PDFs behavior as a function of the Bjorken variable "x" must be determined by means of global fit to the data; this step typically involves simultaneous fit to neutrino data, electron–proton deep inelastic scattering (DIS) measurements, as well as hadron–hadron colliders data.

A number of PDF sets are available from independent global (QCD) fits performed by several groups. The global fits more extensively used by experimental collaborations at LHC include ABKM09/ABM11 [2, 3], CT10 [4], HERA1.5 [5], MSTW2008 [6] and NNPDF2.3 [7]; they are based on different datasets and/or different underlying methodology for treating the data. Many major updates have been recently released, including ABM14 [8] and NNPDF3.0 [10], where updated fit methods, newer datasets and improved theory predictions have been exploited.

The unprecedented center–of–mass–energy available at the Large Hadron Collider (LHC), along with the good angular coverage of the ATLAS detector [9] define a solid ground for constraining the parton distribution functions over a wide kinematical range; the analyses which benefit from improved PDFs knowledge include new–physics searches, Higgs boson measurements and precision electroweak physics.

[a] e-mail: nicola.orlando@cern.ch

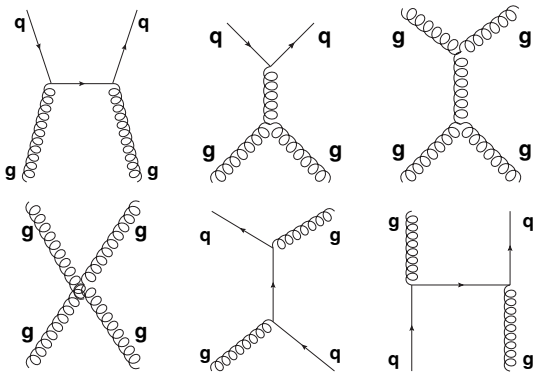

Figure 1. Main Feynman diagrams for describing jet production at LHC.

Many measurements sensitive to parton distribution functions have been performed in ATLAS; they exploit a broad set of data including jets, photons as well as gauge boson, produced inclusively or produced in association with heavy flavour jets.

ATLAS measurements have been already included in the global fits ABM14, NNPDF3.0 and NNPDF2.3.

The ATLAS jet measurements and their constraints on PDFs are summarised in Sec. 2; PDFs studies using the production cross section of isolated photons are highlighted in Sec. 3; in Sec. 4 the measurement of gauge boson production are discussed; the differential cross sections for top quark pairs production are presented in Sec. 5. Finally, concluding remarks are summarised in Sec. 6.

2 Jet cross sections

Jet cross section measurements are the most exploited experimental tools for constraining the gluon density function at hadron colliders. A precise determination of the the gluon density function at LHC is of great relevance for improving the accuracy of theoretical predictions for a wide

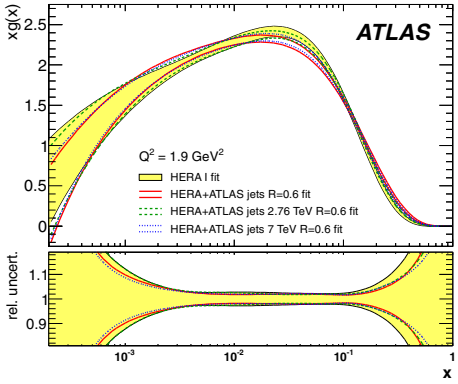

Figure 2. Gluon density function xg(x) and its relative uncertainty shown as a function of x at the scale Q^2 =1.9 GeV^2 [17]. The yellow band indicates a fit to HERA 1 data only. The lines show a fit to HERA 1+ATLAS jet data; the fits to the cross section measurements at center of mass energy of 7 TeV, 2.76 TeV and their ratio is presented separately.

class of processes. In particular, the experimental uncertainty in the gluon PDFs currently dominates the precision of the calculation for the Higgs boson production cross section via gluon–gluon fusion which has been calculated in pQCD up to approximate $O(\alpha_s^5)$ accuracy [11].

As illustrated by the Feynman diagrams in Fig. 1, the main production modes of jets at LHC involve gluons in the initial state; the contribution of Feynman diagrams originating from $q\bar{q}$ scattering are less important due to the suppressed PDFs for anti–quarks.

The use of jet data for PDFs fits is supported by advanced calculations in pQCD. Jets cross section calculations of wide use at LHC are available at next–to–leading order (NLO) for up to three jets in NLOJET++ [12]; electroweak (EW) corrections for jet pair production are also known since more than one decade and have been recently re–evaluated [13]; the residual theoretical perturbative uncertainty form these calculations is estimated to be about 10%. A partial next–to–next–to–leading order (NNLO) calculation for di–jet production at LHC has been recently released [14]; moreover, a new calculation of up to five jets production at NLO has been published [15]; the use of them in future PDF analyses with LHC data is expected to improve the constraints on the gluon PDF and become eventually a standard ground for NNLO QCD fits.

The experimental uncertainty related to jet cross section measurements at LHC is mainly driven by the jet–energy–scale (JES) determination. The JES is calibrated by using a combination of data–driven techniques and test–beam results [16]. For 2011 data sample, the JES has been determined as a function of the transverse momentum and pseudo–rapidity[2] of the jets. The JES uncertainty depends mainly on the jet radius parameter, on the calibration scheme and on the jet p_T and η; for central jets with p_T of about 100 GeV, clustered with the Anti–k_t algorithm and calibrated in the EM+JES scheme, the JES uncertainty is slightly larger than 1%; the JES uncertainty become significantly larger for p_T lower than 20 GeV or higher than 1 TeV where limited data control samples are available for the in–situ JES calibration.

A first inclusive jet cross section measurement sensitive to the gluon parton density function has been performed by using 2011 data [17] at $\sqrt{s}$=7 TeV. The effect of the dominant systematic uncertainties has been mitigated by evaluating the ratio of the measured cross section at $\sqrt{s}$ =7 TeV with the corresponding measurements performed in a smaller data control sample collected at $\sqrt{s}$ =2.76 TeV.

A simultaneous fit to jet ATLAS data and the HERA 1 data has been performed with the HERAFITTER package [18–20] by using a set of PDF parametrisations similar to what has been used in HERA1.5 set [21].

As shown in Fig. 2, the use of ATLAS data in a QCD fit allows for improving the experimental constraints on the gluon density function at high x (x $\simeq$ 0.1–1). Moreover, a harder spectrum of the gluon PDF is observed compared with its previous determination from the HERA 1 data; this feature is more prominent in the data sample collected at 7 TeV.

The new PDF set derived from the simultaneous fit to the ATLAS jet ratio data and HERA 1 data, EPATLJET13, has been used in later ATLAS measurements [22].

Jet production cross sections have been measured in a variety of other topologies, including final states with at least two [22] or at least three [23] high p_T jets; in the former measurement the data have been compared with a QCD NLO calculation and electroweak corrections have been included, while for the latter no electroweak corrections have been used. The electroweak corrections are expected to lower the predicted cross section at high invariant mass of the di– and three–jet systems by a few percents [13]; therefore, their use in future QCD fits using these data will be relevant. All the predictions have been corrected for non–perturbative effects by deriving correction factors with PYTHIA6 [24] and HERWIG++ [25]; the uncertainty on the non–perturbative corrections is estimated to be less than 3% for the di–jet measurement and less than 10% for the three–jet cross sections.

The comparison of the measured cross sections as a function of the di–jet and three–jet invariant mass to the NLO pQCD calculations obtained with various PDFs sets is presented in Fig. 3. Most of the PDF sets describe well the data. The di–jet invariant mass spectrum is well de-

[1]The variable $y^\star$ is evaluated, from the rapidity (y_i) of the selected jets, as:

$$\text{Di–jet:} \quad y^\star = |y_1 - y_2| \,,$$
$$\text{Three–jet:} \quad y^\star = |y_1 - y_2| + |y_2 - y_3| + |y_3 - y_1| \,.$$

[2]ATLAS uses a right–handed coordinate system with its origin at the nominal interaction point (IP) in the centre of the detector and the z–axis along the beam pipe. The x–axis points from the IP to the centre of the LHC ring, and the y–axis points upward. Cylindrical coordinates (r,φ) are used in the transverse plane, φ being the azimuthal angle around the beam pipe. The pseudorapidity is defined in terms of the polar angle θ as $\eta = -\ln[\tan(\theta/2)]$. Transverse momentum and transverse energy are defined as $p_T = p \sin\theta$ and $E_T = E \sin\theta$, respectively.

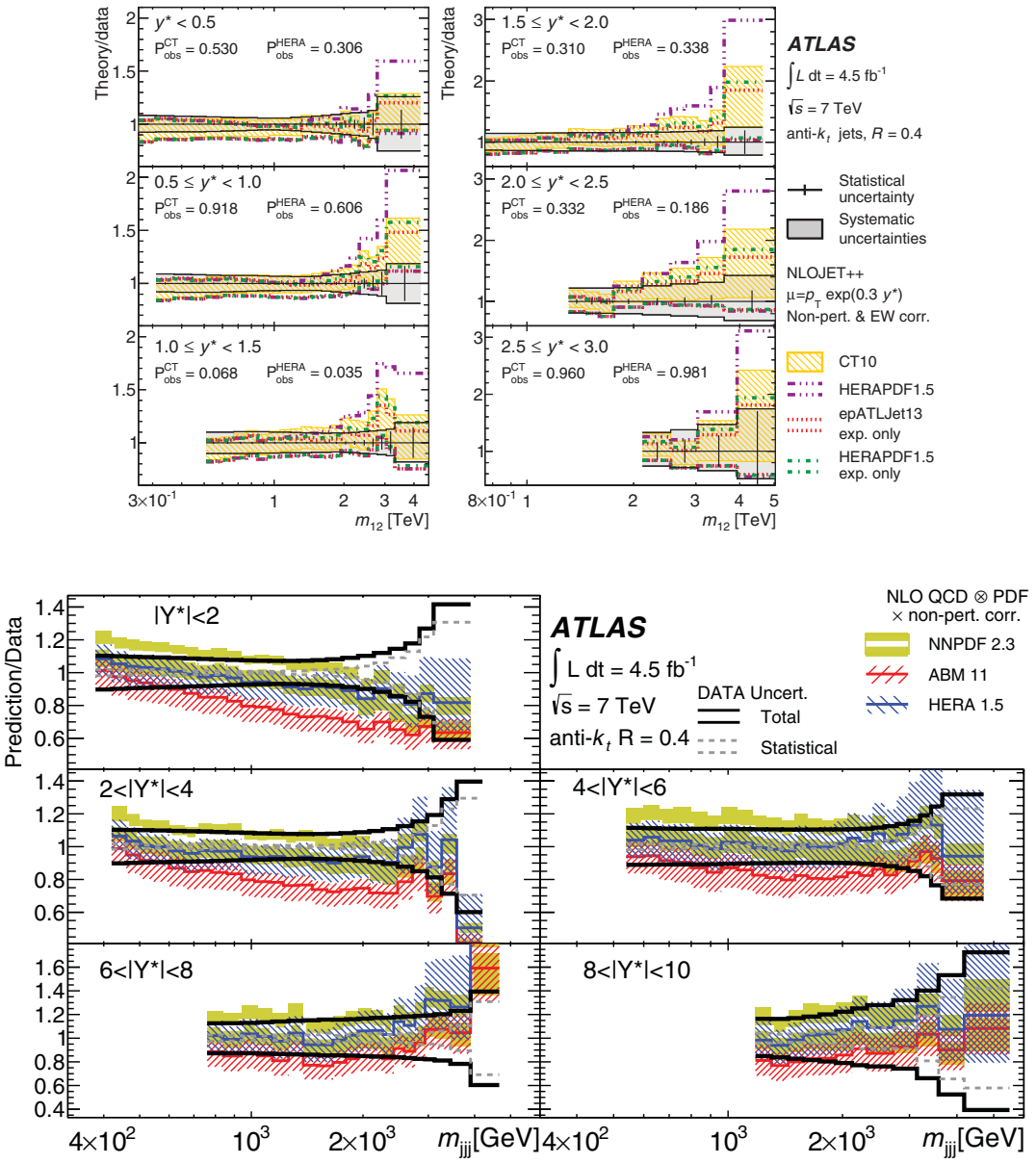

Figure 3. Cross section measurements [22, 23] in various $y^{\star}$[1]regions as a function of the invariant mass of the di–jet (top) and three–jet (bottom) systems. The data are compared to NLO predictions derived with the NLOJET++ generator interfaced with several PDFs sets; NLO electroweak corrections have been applied for the di–jet cross section (top). In each bin the data and the theoretical predictions are divided by the measured cross section. The envelope of the total uncertainty in the measurements is shown by the black solid line; the envelope of the uncertainty on the theory predictions is presented as shaded or hatched bands.

scribed by EPATLJET13; at high invariant mass, the ATLAS PDF set improves the description of the measurement provided by the HERA1.5 set. The ABM11 set, which doesn't include any hadron collider data, provides a poor description of the three–jet invariant mass spectrum.

3 Isolated photons

As illustrated in Fig. 4 (top), photons with transverse energy (E_{γ}^{T}) greater than 100 GeV are produced mostly via (up)quark–gluon compton scattering; this production mode accounts for more than the 65% of the cross section up to E_{γ}^{T}~ 500 GeV. Therefore, measurements of isolated photon production cross section has been advocated as an interesting channel for constraining the gluon density function [26].

As illustrated from the Feynman diagrams in Fig. 4 (bottom), photon production via quark fragmentation provides another production mode at leading order; it comes with larger theoretical uncertainty [27, 28] compared to the prompt photon component.

The most accurate predictions available for inclusive photon production at LHC involve a full NLO calculation of the prompt as well as the fragmentation production

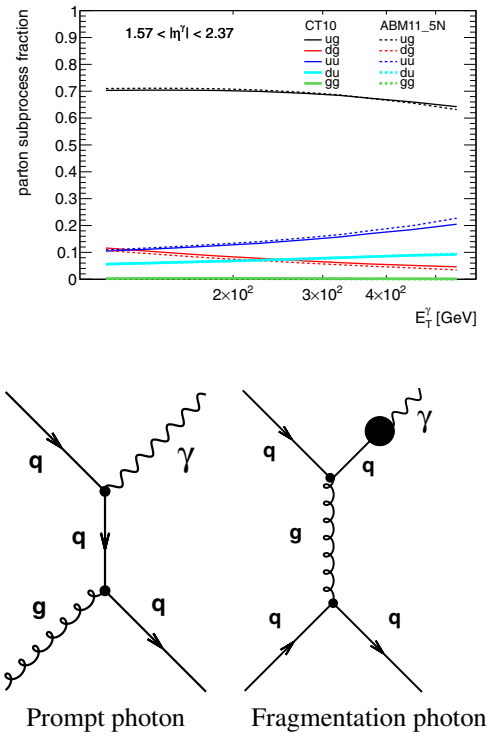

Figure 4. Relative contribution of the inclusive production modes of isolated photons at LHC according to MCFM [30] predictions evaluated as a function of the photon transverse energy (top). Leading order Feynman diagrams for photon production at LHC for the prompt (bottom left) and for the fragmentation (bottom right) components.

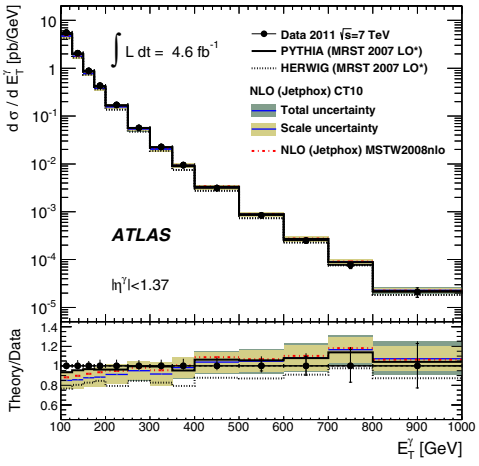

Figure 5. Measured and predicted inclusive prompt photon cross section [29] as a function of the photon transverse energy.

modes [27, 28]; the dominant theoretical uncertainty, of the order of 10% or larger, is driven by the QCD scale (factorisation and renormalisation) variations which are used for evaluating missing higher order in the perturbative expansion of the QCD matrix element and in the DGLAP evolution of the PDFs.

The measured transverse energy spectrum for inclusive isolated photon production [29] is presented in Fig. 5; up to 700 GeV, the experimental precision is significantly better than the precision of the NLO calculation derived with the JETPHOX generator. The main experimental systematic uncertainty is due to the calibration of photon energy scale which amounts to 2–6%.

A comparison of the data to a NLO calculation performed with the MCFM [30] generator is shown in Fig. 6; the MCFM predictions have been derived with a several PDF sets; the ABM11 PDF set is found to provide the best description of the data in spite of not being able to describe well the jet data.

4 Gauge boson production

The identification of gauge boson production in their leptonic decay modes offer a clean experimental handle for studying the quark distribution functions at LHC. Besides, very accurate calculations are available for these processes, including differential NNLO computations in QCD [31–34]; NLO electroweak corrections [35] are also known.

About 20 millions of W bosons decaying in $e\nu_e$ or $\mu\nu_\mu$ leptons and about 2 millions of Z/γ^* bosons decaying in ee or $\mu\mu$ pairs have been collected during the 2011 data taking in ATLAS. The high statistics of W/Z bosons in the 2011 dataset allows for a precise measurements of many experimental signatures, including production of W/Z in association with heavy flavour jets.

A first QCD analysis of the W/Z cross sections measured by ATLAS using the 2010 dataset has been exploited for constraining the strange quark content of the proton [21]. The fit of the strange quark density has been observed to be consistent with unsuppressed strangeness scenario.

The neutral current Drell–Yan (NCDY) process has been measured as a function of the di–lepton, $\ell\ell$ ($\ell = e/\mu$), invariant mass in the range 16–66 GeV and 116–1500 GeV with the full 2011 data sample [36, 37]. These kinematic regions are expected to be sensitive to a different mixture of initial state quarks and to probe a complementary Q^2–x region compared to the "on–peak" Drell–Yan data. At low di–lepton invariant mass ($26 < m_{\ell\ell}[\text{GeV}] < 31$) the uncertainty on the measurement is driven by the systematic errors; the dominant one, of about 3.9%, is due to the multijet background estimation; the statistical error is less than 2% in all the analysis bins. At higher di–lepton invariant mass, $m_{\ell\ell} \geq 400$ GeV, the statistical uncertainty dominates the experimental accuracy; for $m_{\ell\ell}$ larger than one TeV, the statistical uncertainty is 50%.

The NCDY data has been compared to a few theoretical predictions. In order to describe the cross section in the full measured range a NNLO QCD calculation supplemented by NLO EW corrections is necessary; at low di–lepton invariant mass, the NLO QCD calculations, with or without the parton shower, deviate significantly from the data.

The NCDY cross section has a contribution due lepton pairs production from photon–photon scattering; at high di–lepton invariant mass it can be as large as the PDF

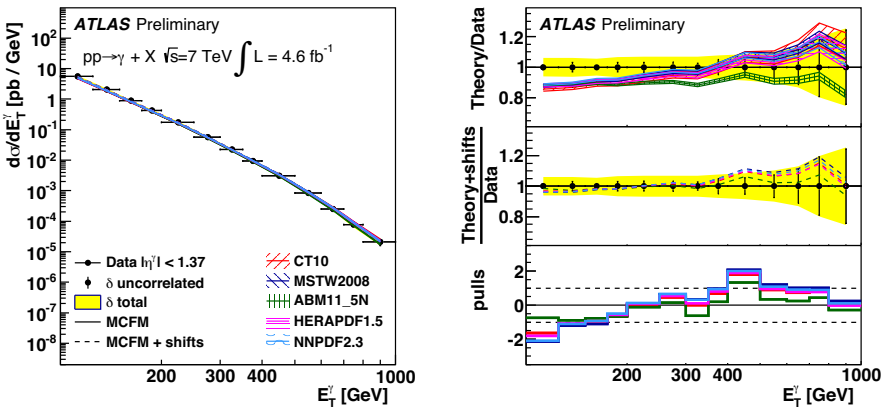

Figure 6. Measured cross sections as a function of photon transverse energy compared to the NLO MCFM predictions derived with different PDF sets. The top right panel shows the ratio of theory to data; the middle panel shows the ratio of theory to data with predictions shifted by the experimental and PDF uncertainties; the lower right panel shows the contribution to the χ^2 of each bin.

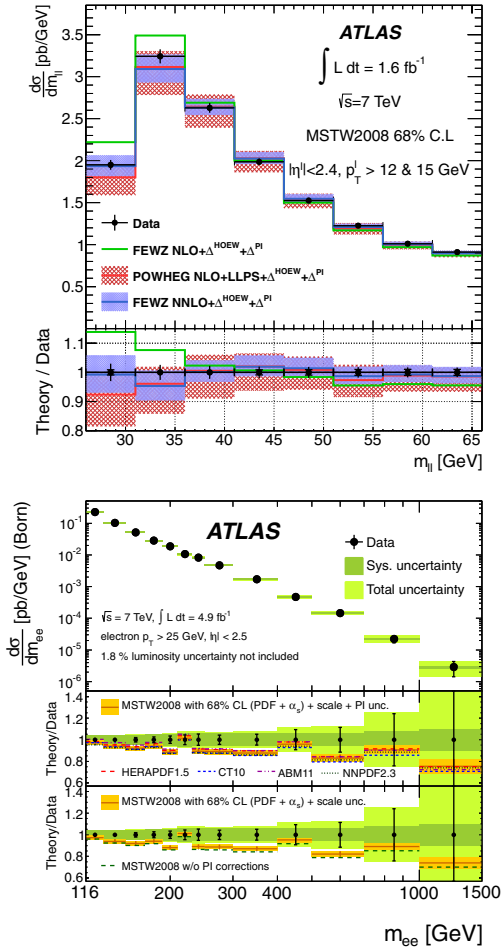

Figure 7. Measured differential cross section for the neutral current Drell–Yan process as a function of the di–lepton invariant mass $m_{\ell\ell}$ at the top (bottom) in the invariant mass range 26–66 GeV (116–1500 GeV). The data are compared to QCD calculation at NNLO, NLO, and to a NLO matched to a parton shower. All calculations are supplemented by higher order electroweak corrections (HOEW) as well as by photon induced (PI) di–lepton production.

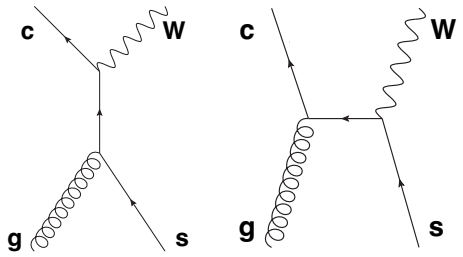

Figure 8. Main Feynman diagrams for W+charm production at LHC; the production modes with a d–quark in the initial state are CKM suppressed, thus they are not shown.

uncertainty of the theory predictions. Indeed, this measurement has shown sensitivity for constraining the photon parton distribution function, as pointed out in the analysis presented in Ref. [38].

The measured NCDY spectrum as a function of the di–lepton invariant mass is shown in Fig. 7 for both the low mass (top) and the high mass (bottom) regions.

Measurements of gauge boson production in association with heavy flavours have been recently published by ATLAS [39, 40].

The W+charm is produced at leading order via s–channel and u–channel production modes involving strange quark–gluon scattering (Fig. 8); thus, a measurement of the W+charm cross section can provide a direct constraint on the strange quark content of the proton. The Feynman diagrams involving a d–quark in the initial state are CKM suppressed, they are expected to contribute by about 10% [41] to the total W+charm cross section. The gluon splitting production modes, along with the most relevant backgrounds, can be suppressed exploiting the charge correlation between the W boson and the charm quark. The total fiducial and differential W+charm production cross sections have been measured [39] by using inclusive charmed hadrons decays into a soft muon as

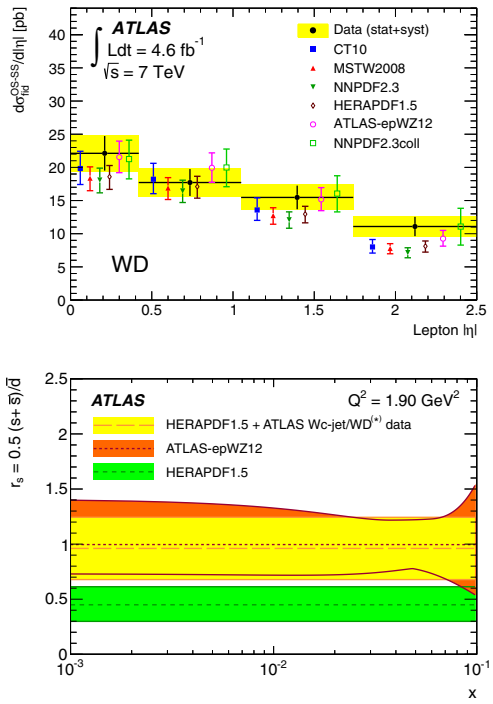

Figure 9. Measured cross section as a function of the lepton $|\eta|$ compared to NLO QCD predictions derived with the aMC@NLO generator interfaced with different PDF sets (top). Ratio of strange-to-down sea-quark distributions $r_s = 0.5(s + \bar{s})/\bar{d}$ as a function of x measured with the fit to the HERA1.5 PDF supplemented by the ATLAS W+charm data. The result is compared to the HERA1.5 and to ATLAS-epWZ12 PDFs (bottom).

well as reconstructing D–mesons in several fully hadronic exclusive decays; an example of differential cross section measurement is shown in Fig. 9 (top), where the data have been compared to a NLO calculation performed with aMC@NLO [42] interfaced with several PDF sets.

The measured W+charm cross sections along with the HERA 1 data have been used for constraining the strange quark PDF in a simultaneous fit; the fit procedure exploits the strange–quark parametrisation available in the HERA1.5 set as a single nuisance parameter, independent on the Bjorken x. The results, presented in Fig. 9 (bottom), favor the unsuppressed strangeness scenario consistently with the inclusive ATLAS W/Z 2010 data analysis [21].

Besides the W+charm cross section measurements, ATLAS presented recently a first detailed analysis of the Z boson production in association with at least one or at least two b–jets (Z+b and Z+bb, respectively, collectively referred to as Z+b(b)).

The phenomenological description of Z+b(b) production at hadron collider has been actively developed during the past decade [43]. Two main theoretical approaches for deriving cross section calculations for the Z+b (and Z+bb) process have been developed[3]:

- Four flavour number scheme (4FNS): b–quarks are generated via initial state gluon splitting described by the fixed–order QCD matrix element.
- Five flavour number scheme (5FNS): b–quarks are generated by the DGLAP evolution of the gluon density function.

In the 5FNS, the main mechanisms for producing a Z boson in association with at least one b–quark involve a scattering between a gluon and a b–quark. Therefore, the Z+b cross section measurement can be exploited for studying the b–quark distribution function. The b–PDF plays a relevant role in t–channel single top production [44], Beyond Standard Model (BSM) phenomenology [45, 46] and electroweak physics [47, 48].

The production of heavy flavours in association with a Z gauge boson is subject to sizable uncertainty on both the experimental and theoretical sides. The experimental uncertainties are mostly driven by the use of the b–tagging, for the Z+b measurement, and limited statistics, for Z+bb. For a final state with at least one b–jet the uncertainty due to the b–tagging is about 6% while the statistical uncertainty on the total cross section is about 1.5%; for a final state with at least two b–jets, the b–tagging uncertainty can become twice larger and the statistical uncertainty on the total cross section is about 4%. The theoretical errors are also significantly larger compared to the inclusive Z boson cross section calculations; the Z+b and Z+bb production are known only at NLO in QCD with or without parton shower in MCFM and aMC@NLO, respectively; predictions based on leading order multileg QCD matrix element merged to a parton shower are also available from several Monte Carlo event generators [49–51]. The uncertainty on the NLO prediction for the Z+b and Z+bb cross sections is between 12% and 17% dominated by the QCD scale variations.

The total fiducial Z+b cross section measurement by ATLAS is shown in Fig. 10 (top) while the differential cross section as a function of the Z boson rapidity is presented in Fig. 10 (bottom). The data have been compared to NLO predictions derived in both 4FNS and 5FNS. In particular, a NLO prediction derived with MCFM in 5FNS has been interfaced with a few PDF sets; the relative variation of the MCFM predictions is observed to be as large as the total uncertainty on the data.

5 Top quark differential cross sections

The use of the top–quark pair ($t\bar{t}$) production cross section for probing the gluon PDF has been recently proposed [52].

The total $t\bar{t}$ cross section is known up to NNLO in pQCD [53]; for $\sqrt{s}$= 7 TeV, the theoretical uncertainty affecting this calculation is about 10%; a preliminary estimation of the differential cross section at NNLO is underway [54]. Other predictions for the differential $t\bar{t}$ cross sections are based on fixed–order NLO in MCFM , NLO matched to a parton shower [55, 56], and LO multileg merged to a parton shower [49].

[3] A more rigorous classification is presented in [43]

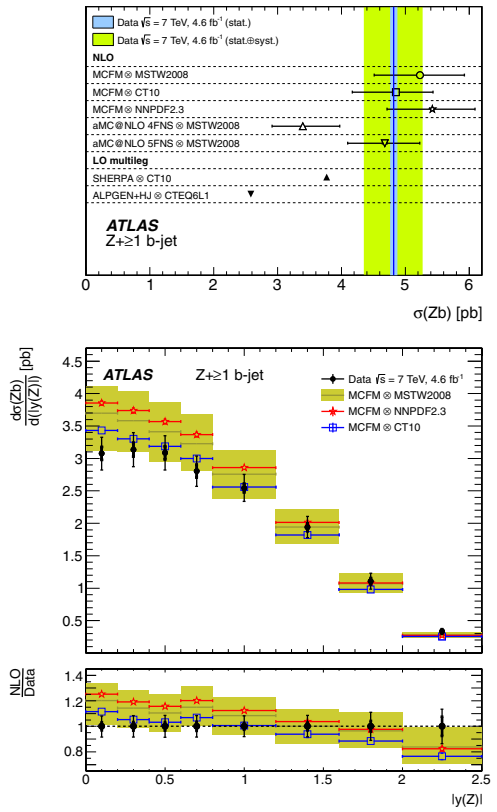

Figure 10. Measurement of the total fiducial cross sections for Z+ ≥ 1 b–jet (top) and differential measurement as a function of the Z boson rapidity (bottom).

Differential $t\bar{t}$ cross section measurements have been published by ATLAS [57]; in Fig 11 the cross section measurement as a function of the $t\bar{t}$ invariant mass is shown. The data are compared to theoretical predictions based on a NLO QCD calculation evaluated with a few PDF sets; only the HERA1.5 set describes well the data, while all the other PDF sets, tuned to Tevatron and/or to LHC jet data, predict a significantly harder spectrum. None of the predictions include EW corrections, which are expected to soften the invariant mass spectrum by a few percents above one TeV.

6 Conclusions

The ATLAS data show clear sensitivity to the proton parton distribution functions and can improve substantially the existing experimental constraints. Simultaneous fits to the ATLAS cross section measurements and HERA 1 data have been performed for improving the experimental knowledge on the gluon and on the strange–quark parton distribution functions.

In order to fully exploit the ATLAS data, advanced theory calculations have been used; next–to–next–to–leading order QCD and next–to–leading order electroweak accuracy are typically needed for a proper interpretation of the data in QCD fits.

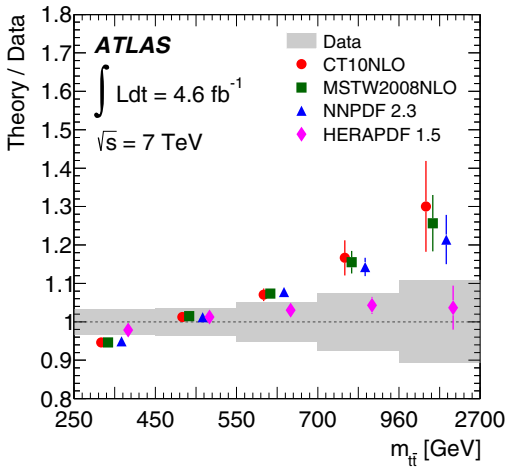

Figure 11. Ratios of the NLO QCD predictions derived with MCFM to the measured normalized differential cross–section as a function of the $t\bar{t}$ invariant mass for different PDF sets.

References

[1] G. F. Sterman, In *Boulder 1995, QCD and beyond* 327-406 [hep-ph/9606312].

[2] S. Alekhin, J. Blumlein, S. Klein and S. Moch, Phys. Rev. D **81** (2010) 014032 [arXiv:0908.2766 [hep-ph]].

[3] S. Alekhin, J. Blumlein and S. Moch, Phys. Rev. D **86** (2012) 054009 [arXiv:1202.2281 [hep-ph]].

[4] H. L. Lai, M. Guzzi, J. Huston, Z. Li, P. M. Nadolsky, J. Pumplin and C.-P. Yuan, Phys. Rev. D **82** (2010) 074024 [arXiv:1007.2241 [hep-ph]].

[5] H1 and ZEUS collaboration, HERAPDF 1.5, H1prelim-10-142, ZEUS-prel-10-018. http://www.desy.de/h1zeus/combined_results/index.php?do=proton_structure.

[6] A. D. Martin, W. J. Stirling, R. S. Thorne and G. Watt, Eur. Phys. J. C **64** (2009) 653 [arXiv:0905.3531 [hep-ph]].

[7] R. D. Ball, V. Bertone, S. Carrazza, C. S. Deans, L. Del Debbio, S. Forte, A. Guffanti and N. P. Hartland *et al.*, Nucl. Phys. B **867** (2013) 244 [arXiv:1207.1303 [hep-ph]].

[8] S. Alekhin, J. Bluemlein and S. Moch, Phys. Rev. D **89** (2014) 054028 [arXiv:1310.3059 [hep-ph]].

[9] ATLAS Collaboration, JINST **3** (2008) S08003.

[10] R. D. Ball *et al.* [The NNPDF Collaboration], arXiv:1410.8849 [hep-ph].

[11] C. Anastasiou, C. Duhr, F. Dulat, E. Furlan, T. Gehrmann, F. Herzog and B. Mistlberger, Phys. Lett. B **737** (2014) 325 [arXiv:1403.4616 [hep-ph]].

[12] Z. Nagy, Phys. Rev. D **68** (2003) 094002 [hep-ph/0307268].

[13] S. Dittmaier, A. Huss and C. Speckner, JHEP **1211** (2012) 095 [arXiv:1210.0438 [hep-ph]].

[14] J. Currie, A. Gehrmann-De Ridder, E. W. N. Glover and J. Pires, JHEP **1401** (2014) 110 [arXiv:1310.3993 [hep-ph]].

[15] S. Badger, B. Biedermann, P. Uwer and V. Yundin, Phys. Rev. D **89** (2014) 034019 [arXiv:1309.6585 [hep-ph]].

[16] ATLAS Collaboration, arXiv:1406.0076 [hep-ex].

[17] ATLAS Collaboration, Eur. Phys. J. C **73** (2013) 2509 [arXiv:1304.4739 [hep-ex]].

[18] F. D. Aaron *et al.* [H1 and ZEUS Collaboration], JHEP **1001** (2010) 109 [arXiv:0911.0884 [hep-ex]].

[19] F. D. Aaron *et al.* [H1 Collaboration], Eur. Phys. J. C **64** (2009) 561 [arXiv:0904.3513 [hep-ex]].

[20] HERAFitter, http://projects.hepforge.org/herafitter.

[21] ATLAS Collaboration, Phys. Rev. Lett. **109** (2012) 012001 [arXiv:1203.4051 [hep-ex]].

[22] ATLAS Collaboration, JHEP **1405** (2014) 059 [arXiv:1312.3524 [hep-ex]].

[23] ATLAS Collaboration, arXiv:1411.1855 [hep-ex].

[24] T. Sjostrand, S. Mrenna and P. Z. Skands, JHEP **0605** (2006) 026 [hep-ph/0603175].

[25] M. Bahr, S. Gieseke, M. A. Gigg, D. Grellscheid, K. Hamilton, O. Latunde-Dada, S. Platzer and P. Richardson *et al.*, Eur. Phys. J. C **58** (2008) 639 [arXiv:0803.0883 [hep-ph]].

[26] L. Carminati, G. Costa, D. D'Enterria, I. Koletsou, G. Marchiori, J. Rojo, M. Stockton and F. Tartarelli, Europhys. Lett. **101** (2013) 61002 [arXiv:1212.5511].

[27] S. Catani, M. Fontannaz, J. P. Guillet and E. Pilon, JHEP **0205** (2002) 028 [hep-ph/0204023].

[28] P. Aurenche, M. Fontannaz, J. P. Guillet, E. Pilon and M. Werlen, Phys. Rev. D **73** (2006) 094007 [hep-ph/0602133].

[29] ATLAS Collaboration, Phys. Rev. D **89** (2014) 5, 052004 [arXiv:1311.1440 [hep-ex]].

[30] J. M. Campbell and R. K. Ellis, Nucl. Phys. Proc. Suppl. **205-206** (2010) 10 [arXiv:1007.3492 [hep-ph]].

[31] R. V. Harlander and W. B. Kilgore, Phys. Rev. Lett. **88** (2002) 201801 [hep-ph/0201206].

[32] C. Anastasiou, L. J. Dixon, K. Melnikov and F. Petriello, Phys. Rev. D **69** (2004) 094008 [hep-ph/0312266].

[33] R. Gavin, Y. Li, F. Petriello and S. Quackenbush, Comput. Phys. Commun. **182** (2011) 2388 [arXiv:1011.3540 [hep-ph]].

[34] S. Catani, L. Cieri, G. Ferrera, D. de Florian and M. Grazzini, Phys. Rev. Lett. **103** (2009) 082001 [arXiv:0903.2120 [hep-ph]].

[35] Y. Li and F. Petriello, Phys. Rev. D **86** (2012) 094034 [arXiv:1208.5967 [hep-ph]].

[36] ATLAS Collaboration, JHEP **1406** (2014) 112 [arXiv:1404.1212 [hep-ex]].

[37] ATLAS Collaboration, Phys. Lett. B **725** (2013) 223 [arXiv:1305.4192 [hep-ex]].

[38] R. D. Ball *et al.* [NNPDF Collaboration], Nucl. Phys. B **877** (2013) 290 [arXiv:1308.0598 [hep-ph]].

[39] ATLAS Collaboration, JHEP **1405** (2014) 068 [arXiv:1402.6263 [hep-ex]].

[40] ATLAS Collaboration, JHEP **1410** (2014) 141 [arXiv:1407.3643 [hep-ex]].

[41] W. J. Stirling and E. Vryonidou, Phys. Rev. Lett. **109** (2012) 082002 [arXiv:1203.6781 [hep-ph]].

[42] J. Alwall, R. Frederix, S. Frixione, V. Hirschi, F. Maltoni, O. Mattelaer, H.-S. Shao and T. Stelzer *et al.*, JHEP **1407** (2014) 079 [arXiv:1405.0301 [hep-ph]].

[43] F. Maltoni, G. Ridolfi and M. Ubiali, JHEP **1207** (2012) 022 [Erratum-ibid. **1304** (2013) 095] [arXiv:1203.6393 [hep-ph]].

[44] B. W. Harris, E. Laenen, L. Phaf, Z. Sullivan and S. Weinzierl, Phys. Rev. D **66** (2002) 054024 [hep-ph/0207055].

[45] M. Flechl, R. Klees, M. Kramer, M. Spira and M. Ubiali, arXiv:1409.5615 [hep-ph].

[46] J. Baglio, M. Beccaria, A. Djouadi, G. Macorini, E. Mirabella, N. Orlando, F. M. Renard and C. Verzegnassi, Phys. Lett. B **705** (2011) 212 [arXiv:1109.2420 [hep-ph]].

[47] T. Gehrmann, M. Grazzini, S. Kallweit, P. Maierhöfer, A. von Manteuffel, S. Pozzorini, D. Rathlev and L. Tancredi, arXiv:1408.5243 [hep-ph].

[48] M. Beccaria, N. Orlando, G. Panizzo, F. M. Renard and C. Verzegnassi, Phys. Lett. B **713** (2012) 457 [arXiv:1204.5315 [hep-ph]].

[49] M. L. Mangano, M. Moretti, F. Piccinini, R. Pittau and A. D. Polosa, JHEP **0307** (2003) 001 [hep-ph/0206293].

[50] T. Gleisberg, S. Hoeche, F. Krauss, M. Schonherr, S. Schumann, F. Siegert and J. Winter, JHEP **0902** (2009) 007 [arXiv:0811.4622 [hep-ph]].

[51] J. Alwall, M. Herquet, F. Maltoni, O. Mattelaer and T. Stelzer, JHEP **1106** (2011) 128 [arXiv:1106.0522 [hep-ph]].

[52] M. Czakon, M. L. Mangano, A. Mitov and J. Rojo, JHEP **1307** (2013) 167 [arXiv:1303.7215 [hep-ph]].

[53] M. Czakon, P. Fiedler and A. Mitov, Phys. Rev. Lett. **110** (2013) 252004 [arXiv:1303.6254 [hep-ph]].

[54] M. Czakon, P. Fiedler and A. Mitov, https://indico.cern.ch/event/290408/timetable/#20140926.detailed.

[55] S. Frixione, P. Nason and B. R. Webber, JHEP **0308** (2003) 007 [hep-ph/0305252].

[56] S. Frixione, P. Nason and G. Ridolfi, JHEP **0709** (2007) 126 [arXiv:0707.3088 [hep-ph]].

[57] ATLAS Collaboration, Phys. Rev. D **90** (2014) 072004 [arXiv:1407.0371 [hep-ex]].